*J.-F. Agassant[1], D. R. Arda[2], C. Combeaud[1], A. Merten[3], H. Münstedt[3], M. R. Mackley[2], L. Robert[1], B. Vergnes[1]**

[1] *CEMEF, Ecole des Mines de Paris, Sophia Antipolis, France*
[2] *Department of Chemical Engineering, University of Cambridge, Cambridge, United Kingdom*
[3] *Lehrstuhl für Polymerwerkstoffe, Universität Erlangen–Nürnberg, Erlangen, Germany*

Polymer Processing Extrusion Instabilities and Methods for their Elimination or Minimisation

This paper presents and reviews findings in relation to three key areas where polymer processing instabilities occur. The paper also describes methods that can be utilised to reduce, or eliminate, the particular instability. Using previously published results in each of the three areas and work presented in the paper, physical insight into the three mechanisms is reviewed and compared. Extrusion instabilities develop with increasing extrusion rate and the onset of extrusion instability is often a key limitation to the maximum output of an extrusion line. The sharkskin instability is an exit effect instability that can be modified by changing exit geometries and eliminated using certain additives. The stick-spurt instability is intimately related to wall boundary conditions which can be influenced by certain wall and polymer formulations. Finally volume instabilities occur in the entry region of a die and result in a highly distorted product. The instabilities are related to viscoelastic effects within the die and can be minimised by appropriate die and polymer modification. The paper provides sufficient experimental background to identify the key physical aspects associated with each of the instabilities and this in turn provides insight into the different way each instability occurs and how they can be minimised.

1 Background

This paper is concerned with a range of instabilities that can occur during the extrusion processing of thermoplastics. The issue is of both academic and commercial interest and because of this there is already a substantial literature on the subject, see for example general reviews on polymer instabilities by *Petrie* and *Denn* [1], *Denn* [2], *Larson* [3]. In places however the literature from specific papers on polymer processing instabilities is difficult to follow as there has not been a universal acceptance of classification and naming. In addition there has often not been a consensus in relation to experimental observations, interpretation of results and associated proposed mechanisms. This paper provides a balanced overview of the position together with recent new results. In addition practical ways are described in which some of the instabilities can be eliminated or minimised.

The word "melt fracture" presents difficulties because in the past, different authors have assigned different meanings to the word. The classification of instabilities here has therefore been divided into three broad categories avoiding the use of melt fracture and the general features of the instabilities can be identified from examination of two previously published flow curves as illustrated in Figs. 1 and 2.

Fig. 1 shows a range of instabilities observed for a linear polyethylene as a function of increasing flow rate. At low flow rate the extrudate is initially smooth and considered to be defect free. As the flow rate increases, an initially small scale surface defect occurs and this is now universally accepted as being called a "**sharkskin defect**". This defect forms the first class of defects that are considered. If the flow rate is increased further, the magnitude of the sharkskin defect increases and for some polymers a discontinuity in the flow curve occurs and pressure oscillations develop. When this happens a "**stick-spurt**" instability occurs and this is the second class of defect considered. With a further increase in flow, a so called "superflow" regime may exist where again the extrudate is smooth and defect free. Finally at very high flow rates a "gross melt fracture"

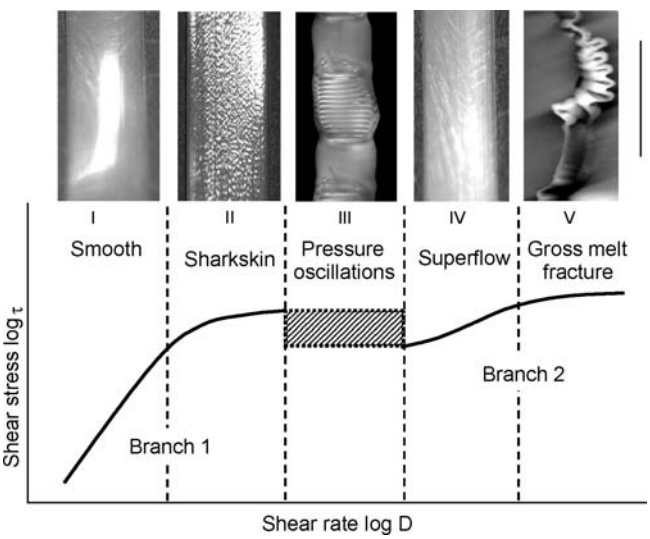

Fig. 1. Examples of different forms of extrusion instabilities seen for linear polyethylene (For details see Merten et al. [21])

* Mail address: B. Vergnes, CEMEF, Ecole des Mines de Paris, UMR CNRS 7635, B.P 207, 06904 Sophia Antipolis, France
E-mail: bruno.vergnes@ensmp.fr

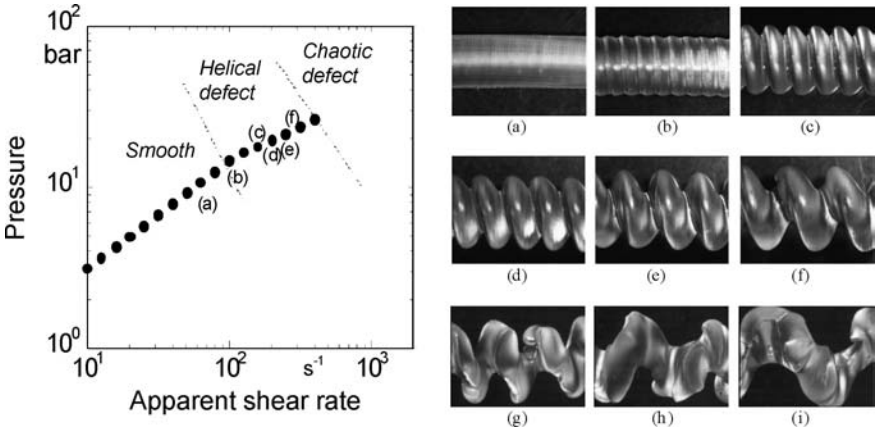

Fig. 2. Examples of upstream instabilities and associated flow curve (For details see Combeaud et al. [72])

region may develop. In this paper gross melt fracture is not examined in detail as the lower flow rate instabilities will limit maximum commercial production rates.

The situation for branched polymers and some other linear polymers can be different to that shown in Fig. 1 and an extrusion sequence for a polystyrene is shown in Fig. 2. For this case the initially smooth extrusion develops a range of periodic instabilities with increasing flow rate, that differ in appearance to both sharkskin and stick-spurt instabilities. These instabilities have in the past been called upstream, volume, reservoir or helical instabilities. In this paper these instabilities have collectively been classified "**volume instabilities**". References relevant to each class of instability will be given in each appropriate section.

The experimental component of this paper draws on an EU consortium project concerned with polymer extrusion instabilities (Postpone Polymer Processing Instabilities 6 5RD-CT-2000-00238). This paper reviews some of the new results obtained within this project and combines this information with existing work in order to reach an overview on each of the three instabilities. The classification into three separate classes of instabilities is by no means exhaustive; however the three separate classes of defect studied here do represent the main instabilities that limit most commercial production of extruded products.

2 Selected Polymers and Experimental Techniques

A series of polymers were carefully chosen in order to demonstrate each particular instability with its greatest clarity and details on the selection of the polymers used is summarised in Table 1. In the case of the **sharkskin instability**, a production linear low density polyethylene (LLDPE) was chosen as commercially this material shows sharkskin and its occurrence limits manufacturing rates. A Repsol, metallocene polymerised

Type of instability	Polymer	M_n M_w kg/kmol	Comment
Sharkskin	Dowlex LLDPE	54800, 113000	Commercial grade
	Repsol mPE	53400, 122,900	Development grade
Stick-Spurt	Dowlex LLDPE	59800, 113000	Commercial grade
	Repsol mPE	53400, 123900	Development grade
	Atofina HDPE	12000, 200000	Commercial grade
Volume	PS	136000, 296000	Commercial grade

Table 1.

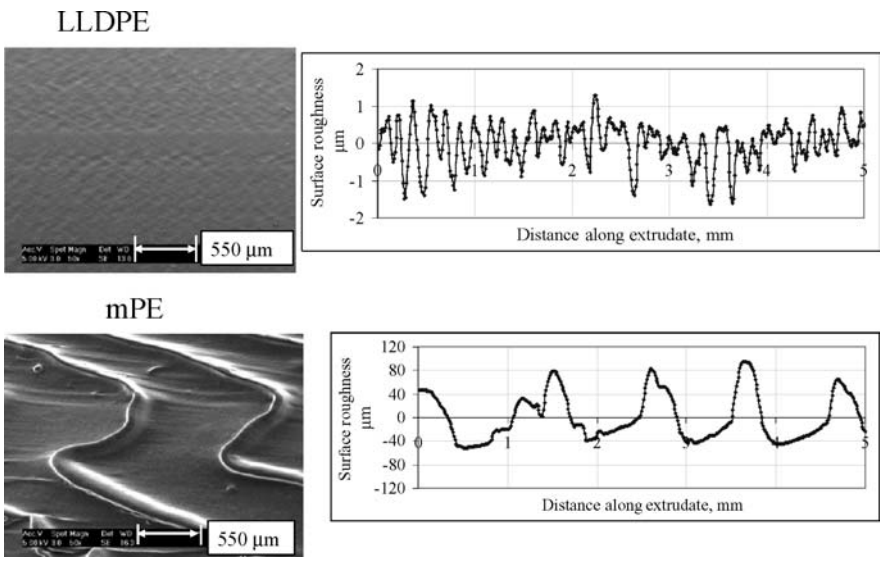

Fig. 3. Examples of sharkskin SEM and surface roughness profiles for LLDPE and mPE (For details see Arda and Mackley [7])

development grade polyethylene (mPE) was also chosen as this material showed very strong sharkskin effects. For the **stick-spurt** instability all the polymers chosen exhibited strong stick slip regions and had similar zero shear rate viscosities. In the case of the **volume instability** a polystyrene grade was chosen as this particular polymer exhibited volume instabilities but not sharkskin or stick-spurt.

Experiments were carried out using a range of apparatus and references are provided that give detailed explanations of each system. In the past it has been generally standard to use pressure drop versus flow rate measurements when examining extrusion instabilities and this technique has been used here and also extended to cover simultaneous pressure readings at different positions within the die. Laser Doppler Velocimetry (LDV) is a powerful probe to measure local velocity measurements and by using test cells with optical windows it has been possible to explore velocity profiles both within and immediately outside the die. The optical transparency of pure polymer melt enables flow induced birefringence (FIB) techniques to be used and this technique has also proved to be powerful for both steady and unsteady flow optical observations. In this case the optical birefringence patterns can be directly coupled with the stress field by use of the linear stress optical law [4].

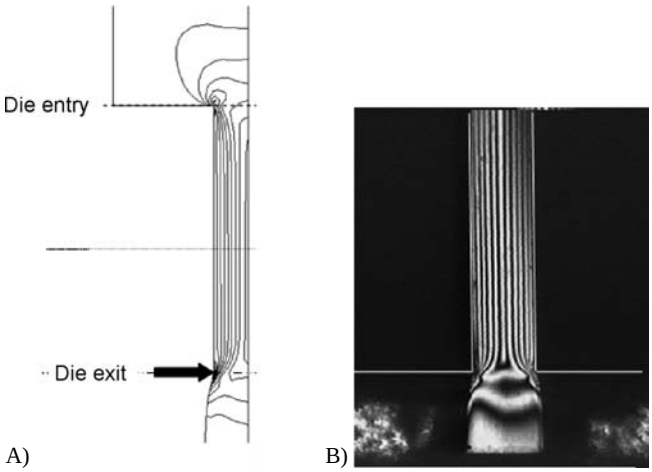

Fig. 4. Example of A) numerical simulation and B) experimental birefringence for LLDPE, illustrating stress concentration at exit of die (For details see Arda and Mackley [7])

3 Sharkskin Extrusion Instabilities

Sharkskin extrusion instabilities develop at certain flow rates for certain polymers and the instability develops as a roughness on the surface of the extrudate [5, 6]. Fig. 3 shows scanning micrographs and matching surface roughness measurements for two polyethylenes illustrating the form of the instability. The surface roughness of the linear low density polyethylene (LLDPE) is mild, but of sufficient magnitude to affect optical properties; the metallocene polyethylene mPE shows a much more severe surface roughness.

It is widely believed that the sharkskin extrusion instability arises from a localized stress concentration at the die exit and in Fig. 4 numerical simulation and experimental flow birefringence photographs show examples of contour plots of principal stress difference within the melt for the LLDPE [7]. Both experiment and simulation indicate that stress concentration occurs at the die exit. Experimentally it is not possible to resolve with absolute confidence the level of stress at the separation point and also the numerical simulation is not accurate at the separation point as it has been established that a mathematical singularity in the stress prediction exists at the point of separation [8, 9].

The detailed mechanism by which the stress concentration at the exit causes sharkskin to occur is still a subject of debate, however the subject can be classified into two main schools of thought.

– Local fracture of polymer at die exit: *Cogswell* [10] proposed that the polymer extrudate fractures at the die exit due to an abrupt change in the flow boundary conditions where the surface layer of the melt accelerates from rest to the average extrusion velocity. The acceleration causes a stretching flow, producing tensile stresses higher than tensile strength that the material can withstand, giving rise to cracking of the surface at the exit, which in turn leads to a momentary relaxation of flow conditions near the edge. This continues in a cyclic manner, giving rise to the sharkskin phenomena. This explanation is consistent with the visual observations made just at the die exit by *El Kissi* and *Piau* [11], who reported the appearance of cracks perpendicular to the flow direction. In addition, *Rutgers* and *Mackley* [12] proposed that a rupture mechanism could explain the correlation between sharkskin and melt strength. *Venet* and *Vergnes* [13] correlate the occurrence of sharkskin with stress levels along local streamlines close to the extrudate surface. The mechanism is further supported by numerous authors and *Allal* et al. [14] have recently proposed a molecular model to describe the periodic fracture effect of polymer downstream of the die exit using this type of concept.
– Local stick slip mechanisms at die exit: *Wang* et al. [15 to 17] explained sharkskin distortions in terms of melt/wall interfacial interactions at a molecular level. Their proposed mechanism states that sharkskin occurs because of a local conformational transition at the die wall exit, where the adsorbed chains become stretched and disentangle with the bulk chains. This layer oscillates between entanglement and disentanglement states due to a reversible coil-stretch transition. The corresponding oscillation of the exit wall boundary condition leads to cycles of local stress relaxation and growth, and to periodic perturbation of the extrudate swell in the form of sharkskin-like surface roughening on the extrudate. Molenaar et al. [18] proposed a local mechanism of stick-slip based on a relaxation oscillation model in a thin peripheral layer near the die exit, similar to the stick spurt instability observed at higher stresses. They modelled melt flow instabilities in terms of cyclic relaxation oscillations, during which potential energy is successively stored and relaxed, and found that above a critical wall shear stress, the increase in the flow curve becomes non-monotonic and successive stick-slip oscillations develop within a localised area at the die exit.

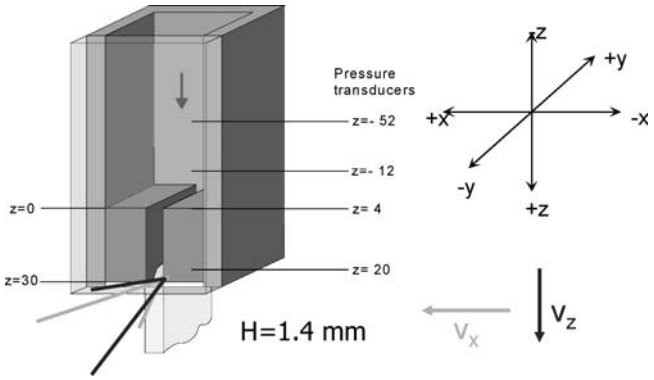

Fig. 5. Schematic diagram of optical slit geometry used in the "Erlangen" experiments. The slit z = 0 mm position was taken at the entrance of the slit and the exit of the slit was at z = 30 mm

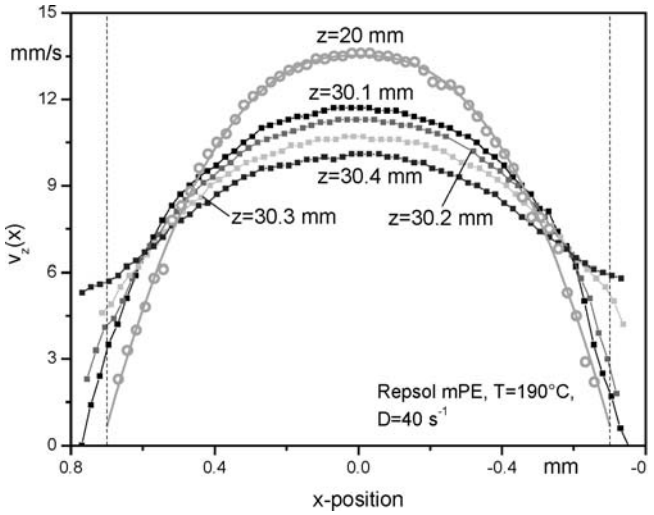

Fig. 6. V_z velocity profiles for mPE flowing within and outside a slit die (For details see Merten [20])

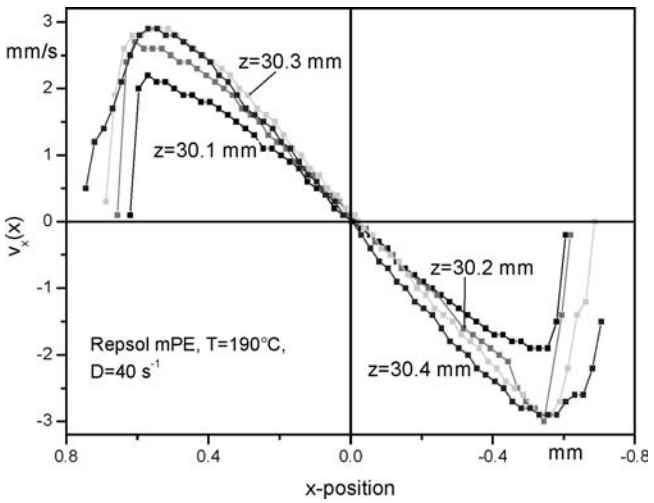

Fig. 7. Horizontal V_x velocity profiles for mPE flowing within and outside a slit die (For details see Merten [20])

3.1 Recent Experimental Observations

Further insight into the mechanism of sharkskin has been obtained from careful laser-Doppler velocimetry measurements [19] and recent results obtained from the University of Erlangen are reported here [20]. Velocity profiles within a slit die containing optically transparent windows were obtained for a flow geometry shown in Fig. 5.

Experimental observation of the mPE in the flow regime where sharkskin is observed shows no detectable pressure fluctuations within the die and also steady birefringence patterns and velocity contours within the slit die. Fig. 6 shows a series of velocity profiles for mPE at different positions within and just outside the slit die. From within the slit at z = 20 mm, a classic "power law" plot can be seen with a near zero velocity at the wall. As soon as the polymer exits the die, for values of *z* higher than 30 mm, extrudate swell occurs and the polymer velocities increase along streamlines near the outer free surface and decrease in the central part of the extrudate. This results in a sharp extensional acceleration for the polymer leaving the die exit. An alternative presentation of this effect is shown in Fig. 7 where the x-component of velocity is plotted downstream of the die exit. A schematic diagram of the situation is shown in Fig. 8, where within the slit, the velocity profile changes at the

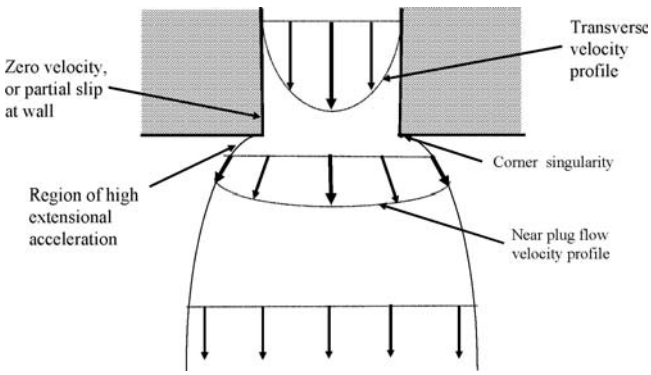

Fig. 8. Schematic diagram of velocity profile rearrangement at the exit of a slit die

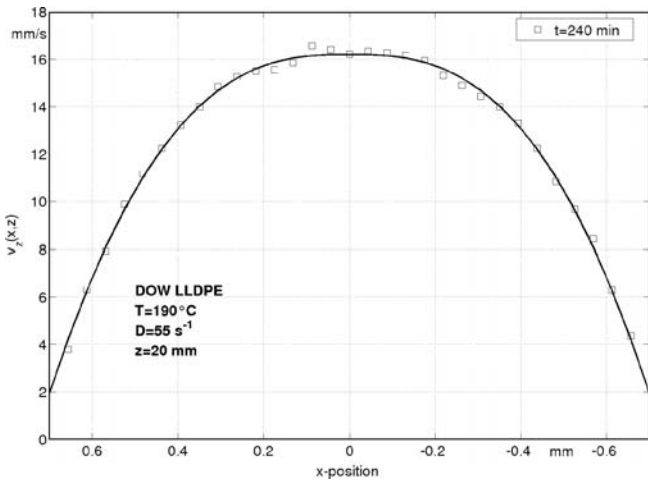

Fig. 9. V_z velocity profiles for LLDPE flowing at z = 20 mm within the slit die (For details see Merten [20])

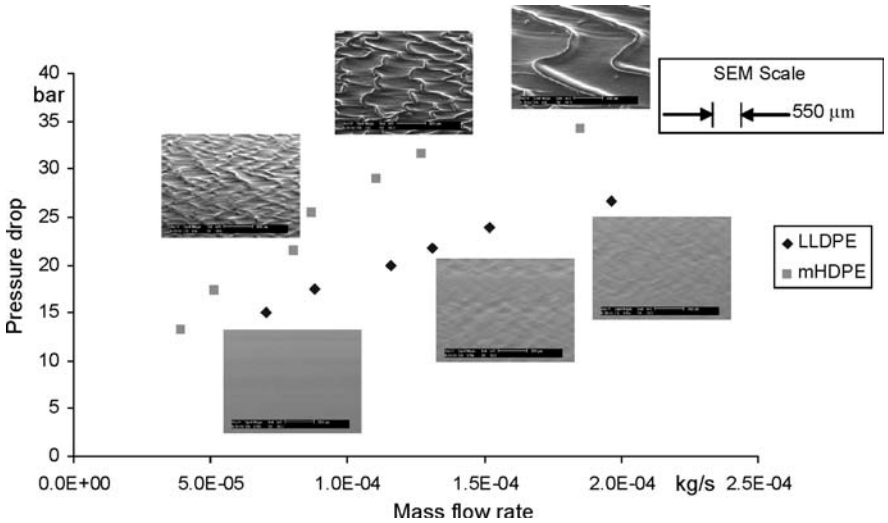

Fig. 10. SEM Photograhs for LLDPE and mPE showing that the magnitude of the instability is greater for mPE than LLDPE at the same extrusion pressure drop (For details see Arda and Mackley [7])

exit into a near plug flow downstream of the exit. The region of high extensional acceleration originating from the separation stagnation singularity at the corner of the die is where the sharkskin instability originates. It is both the localisation and absolute magnitude of the acceleration that combine to give a condition of high stretch and rupture of the material.

Partial wall slip of the polymer will reduce the magnitude of the singularity at the corner, however partial slip may not necessarily eliminate sharkskin. This can be shown for example in Fig. 9 with the LLDPE material where the velocity profile within the slit clearly indicates partial slip. The presence of slip will reduce the stress singularity but, as shown in Fig. 10, the sharkskin instability still occurs, although with less intensity for the same pressure drop than the mPE.

3.2 Methods of Sharkskin Minimisation

The minimisation or elimination of sharkskin is a challenging problem and a number of different approaches have been adopted [22 to 27]. In this paper three different methods are reviewed.

3.2.1 Modification of Die Surface

A number of papers have considered the effect of die surface on sharkskin instabilities and there is general agreement that coatings such as PTFE enhance slip at the wall and thereby reduce or eliminate sharkskin [23, 28]. It has also been found that a coating of the die near the exit is only necessary, again supporting the overwhelming evidence that sharkskin is a die exit effect. Unfortunately PTFE is not sufficiently mechanically stable at polyethylene melt processing temperatures to provide a commercial solution for sharkskin extrusion elimination as within a few hours of operation a PTFE or PTFE coated die will have distorted or have surface damage. As yet, no alternative thermally stable material has been discovered. *Arda* and *Mackley* [29] attempted to introduce gas at the boundary interface of the die in order to develop slip; however they discovered that the separation singularity simply moved upstream to the gas inlet position and sharkskin was not eliminated.

3.2.2 Exit Curvature

A possible way to decrease the stress concentration at the exit of a die is to introduce curvature at the exit [7, 22]. This has been tested and Fig. 11 shows examples of flow birefringence for both a sharp edged exit and a rounded exit profile. In the case of the round edge profile, the point of detachment can occur at different positions along the curved surface and experimentally the detachment point was seen to move downstream from the parallel section of the die. If this situation is simulated for a viscoelastic flow, values of the principal stress difference along a streamline 50 μm from the slit wall and free surface can be generated and these contours are also shown in Fig. 11 below their respective flow geometry. These simulations show that the high stress concentration at the sharp edge exit is greatly reduced if surface curvature is introduced. Experimentally it was found that the introduction of surface curvature did reduce the magnitude of sharkskin but was unable to prevent its appearance. Even when surface curvature is present there will still be a strong extensional acceleration present from the zero velocity separation point as the material accelerates away from the solid surface. The common factor in both cases is the tensile acceleration of the polymer away from the point of separation and it is believed by the authors of this paper that this is the key element for the occurrence of sharkskin.

3.2.3 Effect of Additives

There has been considerable past and recent activity in relation to the elimination of sharkskin by means of polymer additives and at present this is the most effective way to achieve surface defect free extrusions for certain polymers. Most current additives involve the addition of a fluoropolymer additive [28], but more recently Boron Nitride additives [27] and other rubbery polymers [26] have been found to be effective.

An example of the effectiveness of a fluoropolymer additive is shown in Fig. 12. Here surface SEMs and roughness profiles are shown for the mPE at the same extrusion conditions with and without additive. In this case, the results are striking, showing essentially the complete elimination of severe sharkskin.

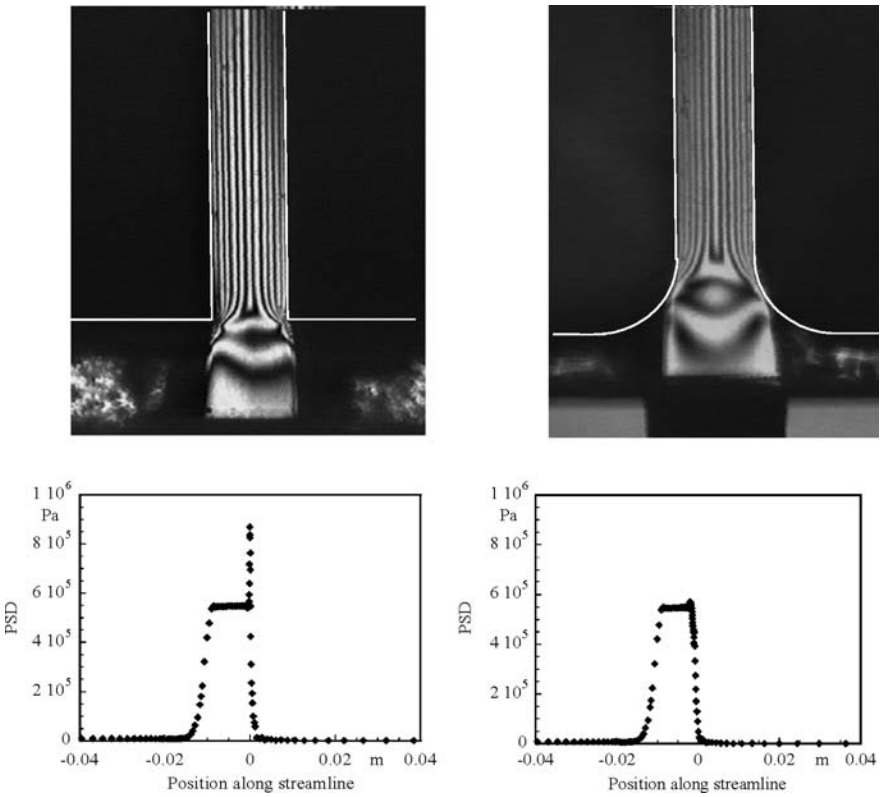

Fig. 11. Effect of die exit curvature on the observed stress field at the exit of a slit flow and also the prediction of Principal Stress Difference profiles along a streamline 50 μm from the slit wall and free surface (For details see Arda and Mackley [7])

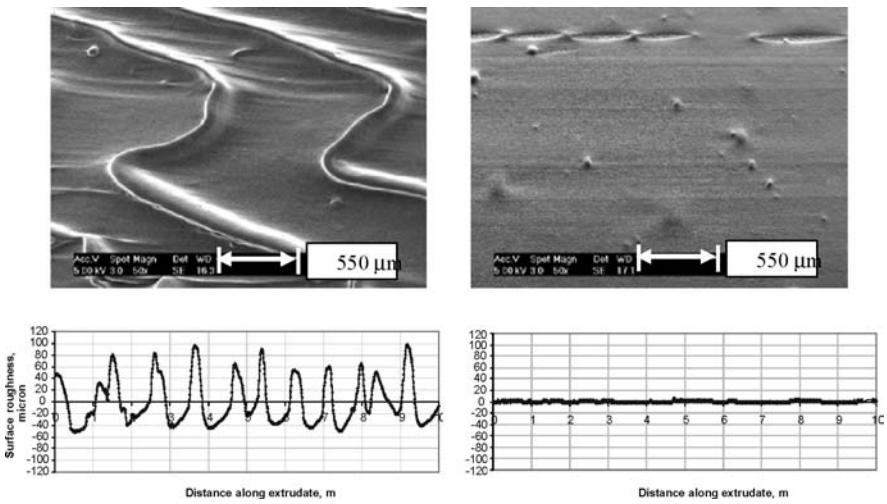

Fig. 12. Effect of additive on sharkskin surface instability for same extrusion conditions. Data on the left hand side additive free, data on the right hand side for polymer containing 1500 ppm fluoropolymer processing aid (For details see Arda and Mackley [7])

There is near universal agreement that processing aids develop a coating at the surface of the die. In a number of cases there can be a time dependence to this coating process and it may take for example an hour for a full coating to develop; in practice this can be achieved more quickly by using an initially high concentration of additive and then reducing the concentration once extrusion conditions have stabilised. In the stable extrusion condition there is compelling evidence to show that partial slip is occurring. Fig. 13 shows the observed extrusion pressures for conditions with and without additive and for the same flow rate the reduced extrusion pressure indicates wall slip. LDV velocity profiles shown in Fig. 14 provide direct evidence that slip is occurring when the fluoropolymer additive is present. The experimental evidence suggests that additives can be effective in providing partial slip and thereby reducing both the magnitude and localisation of velocity and stress concentration in the exit region.

Whilst extrusion additives have been shown to be effective in suppressing sharkskin they have disadvantages in relation to additional cost and also remaining present within the extruded product. There is clearly further scope to develop polymer grades and engineering surfaces that eliminate this type of instability.

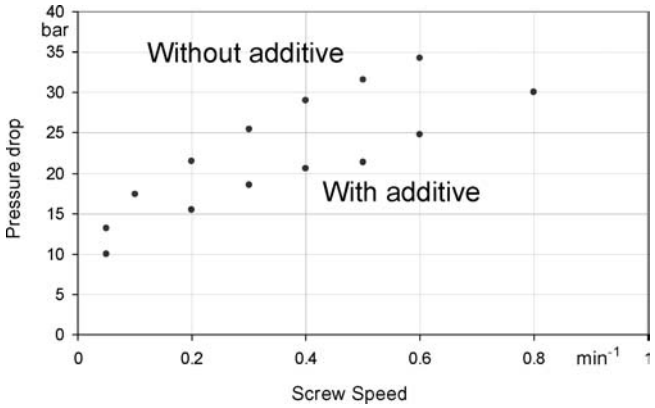

Fig. 13. Effect of additive on extrusion pressure drop for mPE without and with 1500 ppm fluoropolymer processing aid (For details see Arda and Mackley [7])

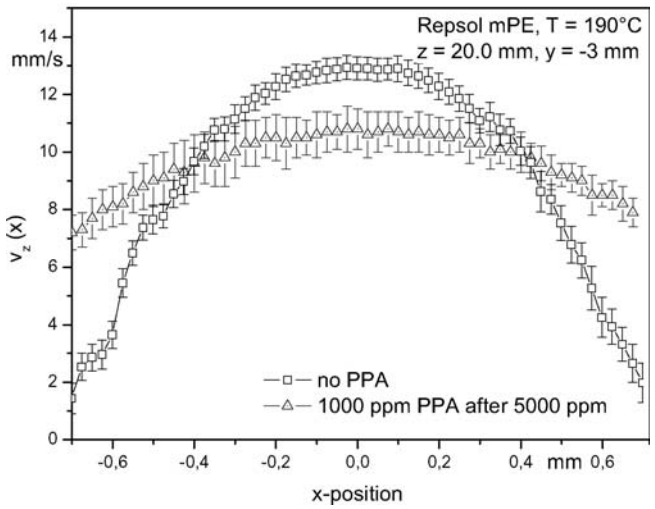

Fig. 14. Effect of additive on velocity profile at the slit die exit for mPE. PPA additive initially applied within polymer at 5000 ppm and subsequently at 1000 ppm (For details see Merten [20])

4 Stick-spurt Extrusion Instabilities

As described in the introduction and shown in Fig. 1, the stick-spurt defect appears particularly for linear polyethylene as a succession of periodic smooth and rough surfaces at an intermediate flow rate range for both high density and linear low density polyethylenes. The rough part of the extrudate surface appearance is similar to the sharkskin defect observed at lower rates and the smooth part of the extrudate is equivalent to that observed in the so called "superflow extrusion conditions" at high rates.

Fig. 15 shows characteristic flow curves for mPE in a capillary rheometer for different L/D ratios. With an orifice die, (L/D ≈ 0), the flow curve is continuous and no pressure oscillation or stick-spurt is detected at any flow rate. However for a non-zero length capillary die, there are two branches to the flow curve; a first branch (branch 1) at low flow rates and a second branch (branch 2) at high rates. Between the two branches, "stick-spurt" pressure and exit flow rate fluctuations occur; if the L/D ratio of the die is increased, the magnitude of the pressure fluctuation increases. This fact, and the disappearance of the pressure oscillation of the orifice die support the assumption of wall slip along the die land as the origin of spurt. The general phenomenon has been extensively studied for constant pressure and constant flow rate upstream boundary conditions and in each case limit cycle oscillations are seen [16, 17, 30 to 35].

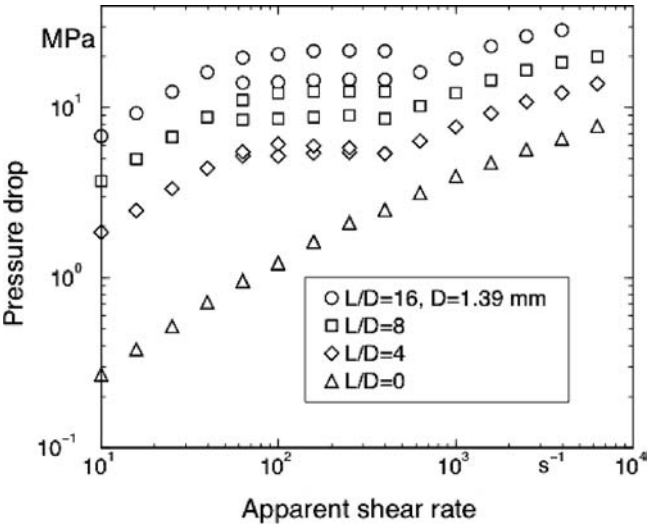

Fig. 15. Flow curves for mPE for different L/D ratios (For details see Robert [38])

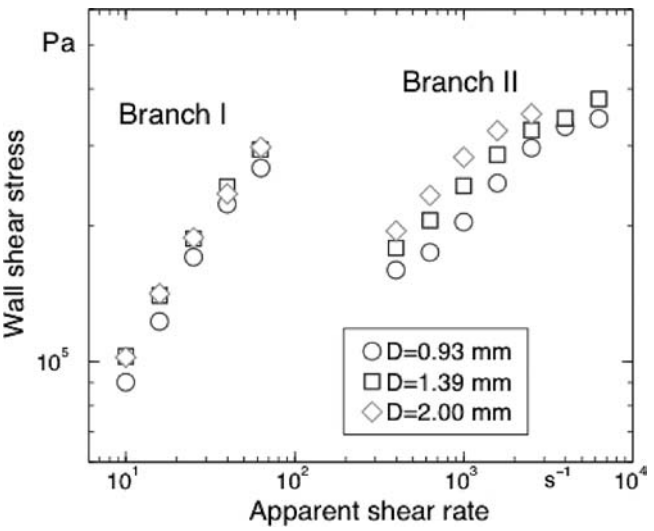

Fig. 16. Flow curves for mPE for different capillary diameters (For details see Robert [38])

Fig. 16 shows the characteristic flow curves for different die diameters. Along branch 1, the flow curve is only slightly dependent on die diameter and indicates no slip or only weak slip at the wall. Along branch 2 there is a strong die diameter dependence which indicates the existence of wall slip. The detailed shape of the pressure trace fluctuations and the coupled behaviour of the exit flow have been studied by amongst others, *Wang* et al. [15], *Hatzikiriakos* and *Dealy* [34] and *Durand* et al. [35]. When the pressure increases in the reser-

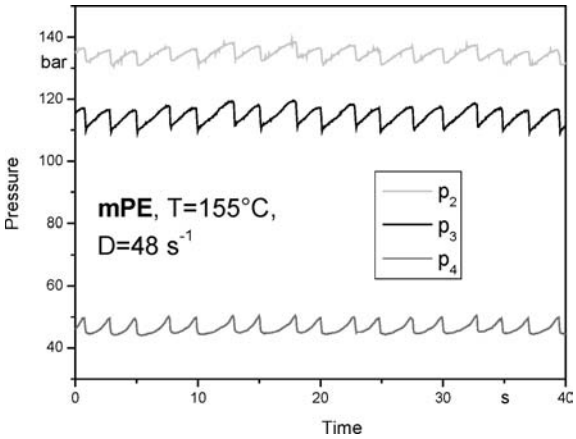

Fig. 17. Pressure fluctuations for mPE at three different positions within slit die (For details see Merten et al. [21])

voir, the die exit velocity is small and the extrudate is rough. When the pressure reaches a critical value, there is a sudden velocity jump followed by a sharp pressure decrease and the extrudate is smooth. Then the pressure starts to increase again and a new cycle is initiated. Both the pressure and exit flow rate fluctuations depend on the upstream volume of the reservoir [35, 36]. All these results are now well established and documented and a number of publications include the application of macroscopic relaxation oscillation models to describe the results. A recent development however has been the direct measurement of coupled pressure, stress and velocity fluctuations within the flow domain and results of this type are reported in the following section.

4.1 Flow Field Investigation within a Slit Die

By using a slit die with optical windows of the type described in section 2, Fig. 5, it was possible to obtain correlated pressure, stress and velocity data for flow within the stick-spurt regime and experimental data, including LDV from CEMEF, Sophia Antipolis, and LSP Erlangen is included in this section.

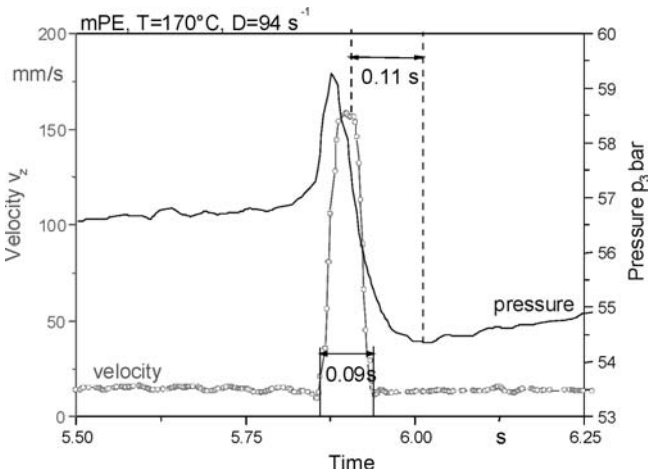

Fig. 18. Pressure and velocity fluctuations for mPE at z = 20 mm (For details see Merten et al. [21])

Fig. 17 shows that pressure fluctuations measured at various positions along the slit ($z = -12$, 4 and 20 shown in Fig. 5), are in phase for the whole flow domain including both the entry and slit region, although the shapes of the pressure transients are different in the different positions. These results demonstrate that the instability does not propagate as wave within the die, as the response is everywhere in phase. Fig. 18 shows a more detailed pressure trace within the die land (z = 20) together with the superimposed centre line velocity as a function of time. In this figure it can be seen that the spurt velocity period occurs immediately after the pressure maximum occurs.

A transparent slit die allows point wise LDV velocity measurements to be made [37] and, by traversing the LDV across a slit, velocity profiles can be obtained. *Robert* et al. [38 to 40] carried out a number of velocity profile measurements and examples of their data are shown in Figs. 19 to 21. The figures show experimental velocity profiles and in some cases, matching numerical simulation for three different flow regimes, namely flow in branch 1, 2 and the intermediate stick-spurt regime. The figures show the velocity profiles across a slit gap for different positions along the slit width. As the flow is symmetrical, only one half of the slit section is shown. Fig. 19 shows the experimental velocity profile and matching numerical simulation for branch 1 of the flow curve and the data show a number of important features. It can be seen that the flow is not two dimensional. This results in different flow profiles throughout the width of the slit and this makes analysis of the flow more difficult than say in a circular capillary. The simulation assumes a no slip boundary condition and for this branch of the flow the assumption is correct. Fig. 20 shows the velocity profile in branch 2 of the flow curve. Here velocities are greater and the velocity profile is much flatter. The match between experiment and simulation is poor, as the simulation still assumes a zero slip boundary condition which is clearly now not correct. Fig. 21 shows the extrema of the velocity profiles in the stick-spurt regime and here the profiles oscillate from the lower, no slip profile, to the higher velocity slip profile. These profiles provide direct evidence that the stick-spurt effect is associated with wall slip at, or very near to the wall surface.

Flow Induced Birefringence (FIB) has been extended to the study of unsteady flows in the stick-spurt regime [39]. Fig. 22 shows a flow birefringence stress field within a slit where the different fringes correspond to different levels of stress at any one instant in time. In the stick-spurt regime these fringes are observed to change with time and this effect is shown in Fig. 23 where contours of stress levels are plotted as a function of time. In Fig. 18 it was seen that the pressure build up to a maximum before the spurt velocity period occurred. Fig. 23 shows that the birefringence peaks after the pressure maximum indicating, initially surprisingly, that pressure and birefringence are not in phase. The reason for this feature relates to the importance of compressibility in the stick-spurt instability. In the pressure build-up phase of the cycle there is little flow and the pressure contribution is related to an increase in hydrostatic pressure within the die. When slip occurs, there is then both a pressure drop and a birefringence contribution due to the flow. Thus in the case of stick-spurt flow pressure and birefringence are not in phase with each other.

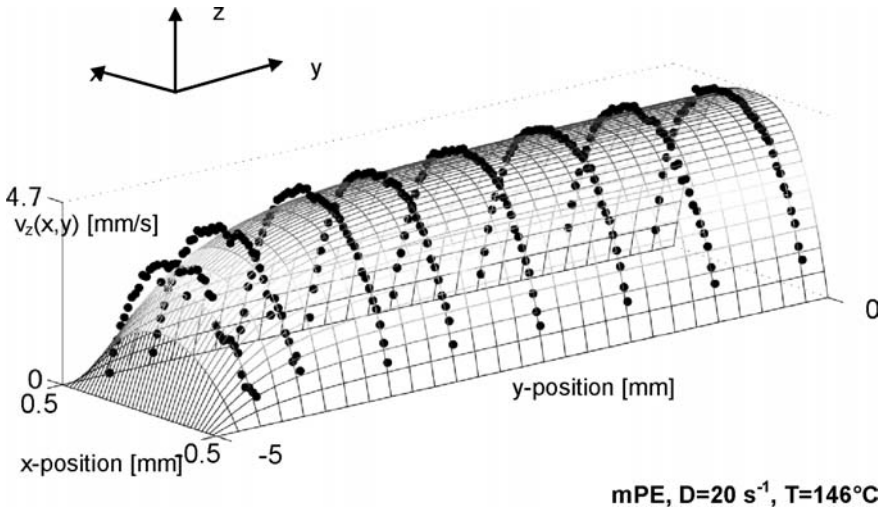

Fig. 19. Velocity profiles and matching numerical simulation in branch 1 region of flow for mPE (For details see Robert et al. [40])

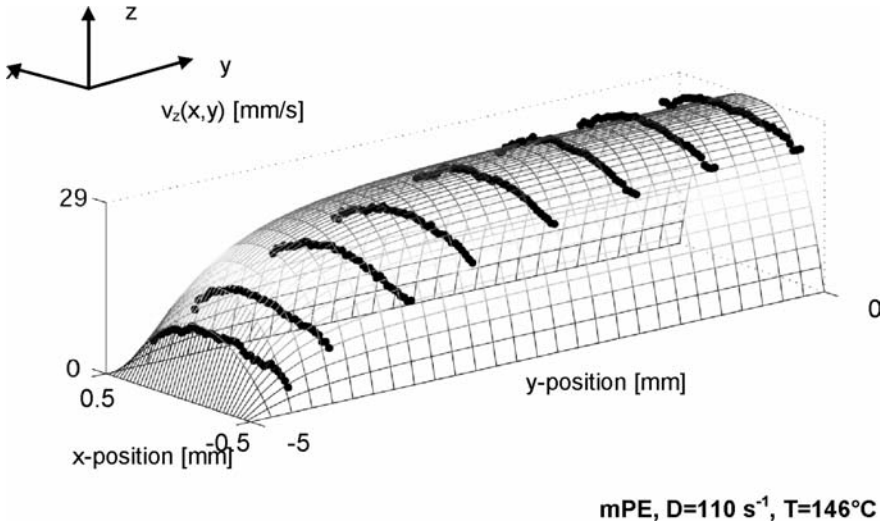

Fig. 20. Velocity profiles and matching numerical simulation in branch 2 region of flow for mPE (For details see Robert et al. [40])

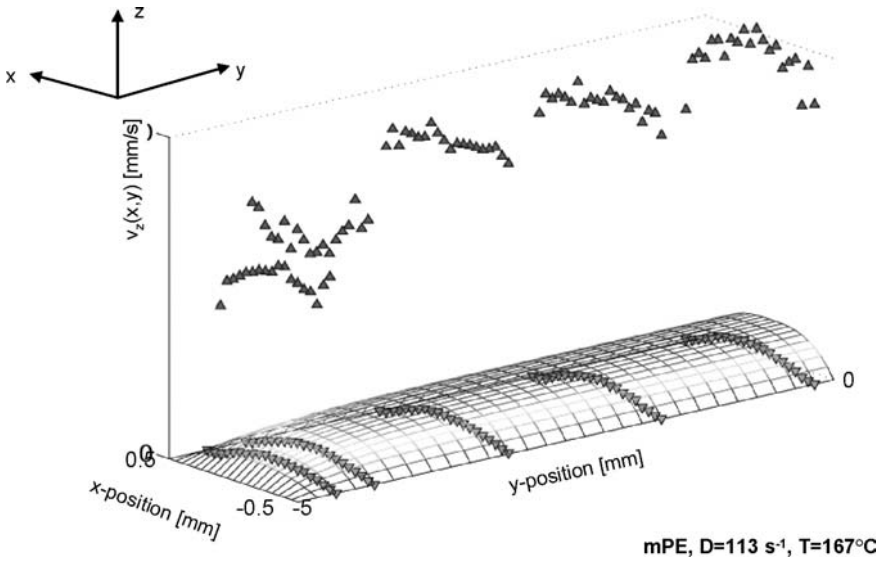

Fig. 21. Velocity profiles and matching numerical simulation in stick-spurt region of flow for mPE (For details see Robert et al. [40])

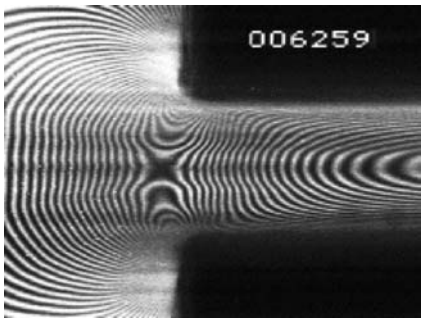

Fig. 22. Typical flow birefringence pattern during stick-spurt region of flow (For details see Robert [38])

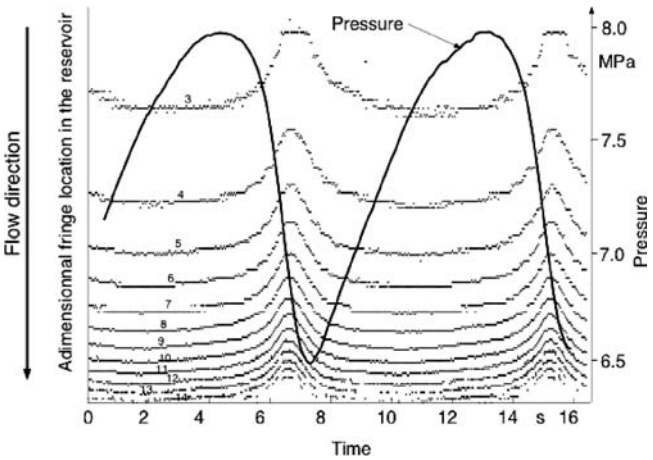

Fig. 23. Reservoir pressure and centre line birefringence variation as a function of time during stick-spurt. The fringe numbers increase from 3 to 14 from upstream of the die entry towards the contraction (For details see Robert et al. [39])

4.2 Key Factors and Mechanisms Controlling the Stick-spurt Instability

From the shape of the pressure trace and the variable mass flow output, it is clear that compressibility must be included in any model that describes stick-spurt. In addition the wall slip and LDV data indicate that variable wall boundary conditions occur during stick-spurt. Both these elements are common to all of the current relaxation oscillation models used to describe stick-spurt although the way the components are introduced is not universal. Most authors introduce compressibility only in the reservoir region of the die [34, 36, 41, 42] and the stick-slip transition may be discontinuous [34, 35] or mild (non monotonous slip law), based on phenomenological equations [43], molecular dynamic [44, 45] or on stochastic desorption mechanisms [46].

The resulting relaxation oscillation models involve solving a compressibility equation in the reservoir coupled with a simple or sophisticated stick-slip transition equation in the die land (see for example *den Doelder* et al. [36]). As shown in Fig. 24 these types of models are able to capture the pressure trace as a function of time at successive shear rates within the spurt regime. Nevertheless, this model is unable to predict the critical shear stress values which initiate the spurt area on the flow curve. In addition these models are only suitable for a capillary rheometer. As pointed out in Figs. 20 and 21, the slip velocity is not necessarily uniform throughout the width of the slit. Finally, these types of model are not able to explain why some polymers exhibit stick-spurt defect and others do not.

As polymer compressibility is usually of the same order of magnitude for different polymer species, the key factor is the wall slip condition where the competition between macromolecule adhesion at the wall and entanglement/disentanglement mechanisms between tethered chains and the untethered bulk polymer chains is crucial. Polystyrene (PS) does not show stick-spurt, but HDPE does. In the case of PS the molecular weight between entanglements is high and for PE it is low. It is unlikely however that this is the only factor that needs to be considered because, for example, different types of polyethylene behave in a different way. Different polymers will also have different tethered chain densities and the chemical nature of the die surface as well as its roughness will influence behaviour. This is an area of modelling that is currently receiving detailed numerical simulation [44, 47].

4.3 The Minimisation of Stick-spurt Defects

The development of understanding relating to the origin of the stick-spurt instability has enabled a number of methods to be introduced to minimise this instability. If no discontinuity in the flow curve exists no stick-spurt will be seen and this for example is the case with PS, some LLDPEs and also LDPE. The stick-spurt instability is sensitive to both L/D ratio and upstream reservoir volume and if both of these parameters are minimised the stick-spurt effect will also be reduced.

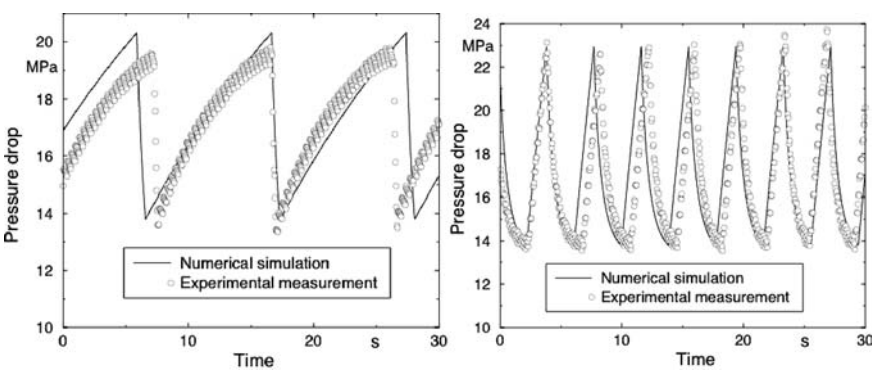

Fig. 24. Matching of pressure fluctuations in stick-spurt flow with model predictions (For details see Robert [38])

It has been reported that the upstream introduction of a packed bed filter is effective in suppressing pressure oscillations [48 to 50], and Fig. 25 shows that the introduction of the filter has eliminated the discontinuity in the flow curve [38]. Elimination of the flow curve discontinuity has eliminated the instability; however the introduction of the filter has resulted in a significant increase in the overall pressure drop for the system.

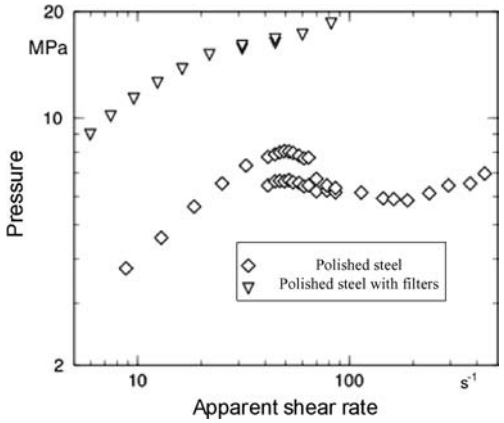

Fig. 25. Effect of filter introduction on flow curve (For details see Robert [38])

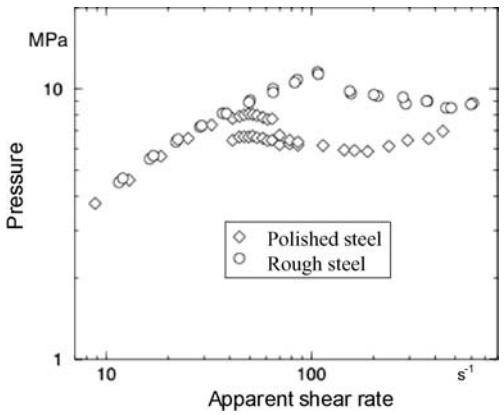

Fig. 26. Effect of surface roughness on flow curves (For details see Robert [38])

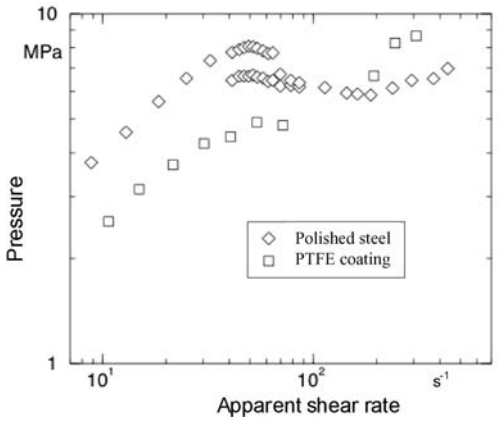

Fig. 27. Effect of surface coating on flow curves (For details see Robert [38])

Because the stick-spurt instability is directly related to wall slip boundary conditions it should be possible to modify both the physical and or chemical nature of the surface and eliminate the instability. Fig. 26 shows that the physical nature of the surface can influence the flow curve and hence the existence of the instability. If the steel surface was smooth the flow discontinuity occurred at a certain apparent shear rate. By roughening the surface the flow curve was modified and the discontinuity was delayed to a higher shear rate. Roughening of the surface influenced the onset of the instability but did not prevent it [17].

There are conflicting reports in the literature on the effect of the chemical nature of the material on stick-spurt. *Ramamurthy* [51] reported differences in stick-spurt behaviour using brass dies and *Ghanta* et al. [25] reported that the effect was very sensitive to both processing and surface treatment protocol. Robert [38] however saw no difference between slit dies made from polished steel and brass. Fig. 27 shows flow curves for a steel and a PTFE coated die where the coating has the effect of reducing the flow discontinuity and also the stick spurt effect as also reported by *Wang* and *Drda* [17] and *Koran* and *Dealy* [52].

5 Volume Extrusion Instabilities

The development of periodic bulk instabilities affecting extrudates are observed classically for branched polymers (low density polyethylene), and in some cases also for elastic linear polymers with high normal stresses and long relaxation times (polystyrene, polypropylene). When emerging from a circular die above a critical condition, the extrudate develops a perfect helical shape, as described in the introduction and shown in Fig. 2. As the flow rate increases further, the extrudate progressively loses its periodicity, until it presents gross melt fracture [53]. For similar process conditions, extrudates emerging from a slit die do not exhibit periodic helical distortions, but do exhibit periodic volume distortions. As a result of this, whatever the flow geometry studied, the term "periodic volume instability" will be used. Volume instabilities are instabilities that involve the whole volume of the extrudate, as opposed for example to sharkskin instabilities which are a surface related distortion. Volume instabilities, including gross melt fracture, are instabilities that originate in the upstream region of the extrusion reservoir.

In 1956, *Tordella* [54] explained that the onset of volume instabilities was characterized by a change in the slope of the flow curve for polymers that show a single continuous flow curve. The effect was particularly pronounced for short capillary lengths [55, 56]. Critical parameters usually used to quantify the onset of the upstream instability are the shear flow parameters, such as apparent wall shear rate or wall shear stress [57]. Various experimental techniques have been applied to the study of volume instabilities, including flow birefringence [50, 58], particle tracers [59 to 61], laser-Doppler velocimetry (LDV) [61, 62] and Particle Image Velocimetry (PIV) [63]. All these experimental observations have shown that the upstream contraction region of the flow was the site of the in-

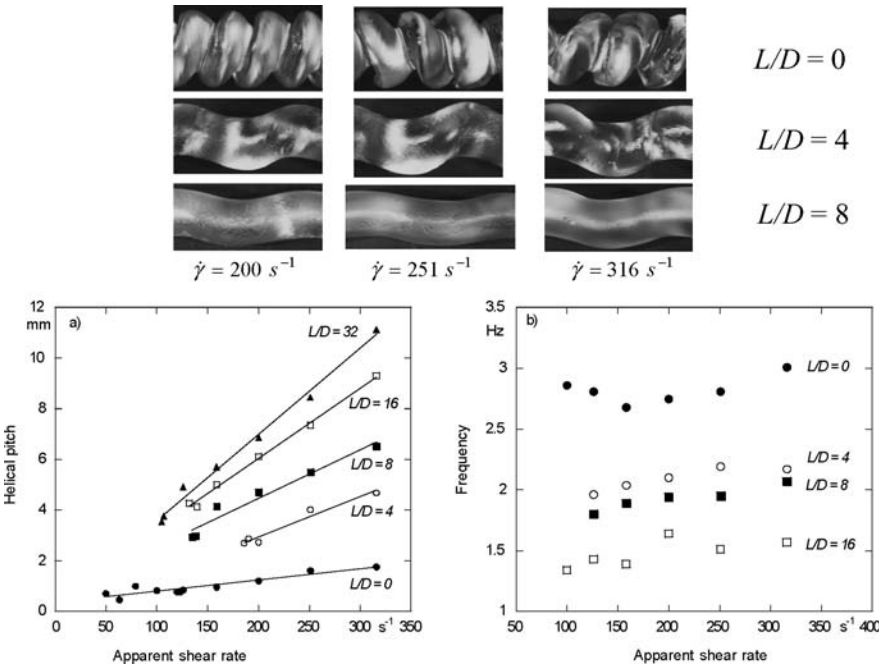

Fig. 28. The effect of apparent shear rate and L/D on volume instabilities for polystyrene (For details see Combeaud et al. [53])

stability initiation. The capillary inlet is a region where the fluid is submitted to high elongational deformations and this extensional flow plays an important role in upstream instabilities. Generally previous studies have indicated that both entry recirculation and viscoelastic fluid properties coupled to the flow geometry are responsible for the occurrence of volume instabilities; however for certain polymers *Kim* and *Dealy* [64, 65] have recently proposed a critical tensile stress as a criterion for the onset of volume instabilities involving gross melt fracture. They argue that gross melt fracture would involve the true fracture (rupture) of the melt, specifying that it may be the result of chain scission or sudden disentanglement and chain pull-out.

5.1 Capillary Rheometer Results

Insight into the helical volume instability can be obtained from correlation of the nature of the extrudate and the materials flow curve. Fig. 2 shows an apparent flow curve for Polystyrene obtained at a temperature of 200 °C with a capillary diameter of 1.39 mm. The flow curve (pressure as a function of the apparent shear rate) was continuous and showed different zones, with various extrudate regions (separated by dashed lines on the graph). At low shear rates (in the range 100 to 150 s^{-1}), the extrudate was perfectly smooth (photograph 2a). Above a critical shear rate, a helical extrudate developed (photograph 2b). When flow rate increased further, the helix became more and more pronounced (photographs 2c–f), affecting all the extrudate volume (helical pitch and diameter increase with flow rate). For apparent shear rates higher than 400 s^{-1}, a degradation of the helix was observed (with a loss of perfect periodicity, photograph 2g), followed by the progressive transition towards a chaotic instabilitiy (photographs 2h–i). As described in the literature [56, 66, 67], the onset of the helical defect is characterized by a change in the slope of the flow curve which is well pronounced as in the case of small L/D ratios shown in Fig. 2.

Fig. 28 shows a series of photographs and data where the effect of apparent shear rate and L/D ratio of the die was investigated for a capillary die. The periodic volume instability has a characteristic frequency [53, 68] and the frequency is not very sensitive to the apparent shear rate as shown in the figure. For a fixed geometry, the instability develops with a constant frequency and with growing helical volume distortions. If the length of the capillary is considered, it has also been shown that the frequency increases as the capillary length decreases [53] and this in turn means that the pitch of the instability increases with increasing L/D also as shown in the figure. This general qualitative feature was first reported by *Bergem* [69] and subsequently by others [70, 71]. If the volume/cycle of the instability is taken into account, for a given flow rate, the volume in cycle will increase with increasing L/D ratio.

5.2 Flow Birefringence and Velocity Fields within the Entry of a Slit Die

Whilst it is convenient to study the systematic downstream evolution of helical instabilities in a cylindrical die, it is difficult to study the exact upstream behaviour of the material within the entrance region of the die. Slit dies however provide an excellent opportunity to observe upstream behaviour using both flow birefringence (FIB) and laser-Doppler velocimetry (LDV), although the systematic downstream evolutions of the instabilities are less clearly presented. In terms of visualisation, Fig. 29 shows the apparent flow curve for polystyrene at a temperature of 180 °C and the associated upstream flow induced birefringence (FIB) patterns for the case of an abrupt slit contraction [72].

The isochromatic fringes corresponding to Fig. 29A are stationary: with time; however as the apparent wall shear rate

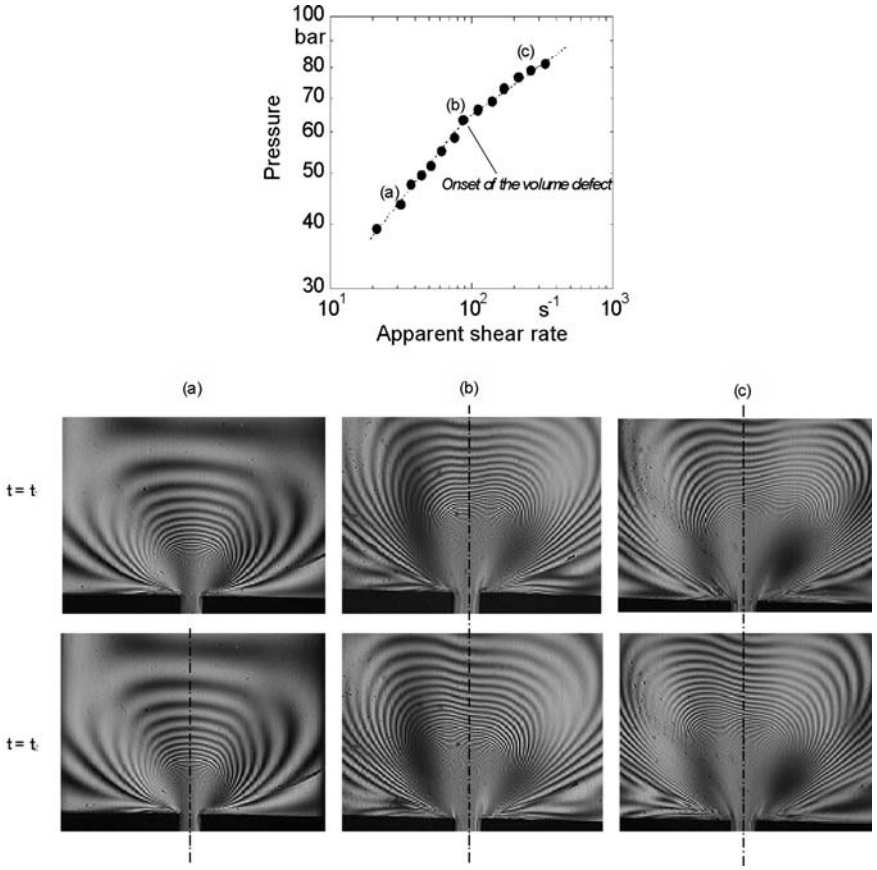

Fig. 29. Apparent flow curve and associated FIB patterns (a): 30 s^{-1}, (b): 87 s^{-1}, (c): 263 s^{-1} (abrupt contraction, T = 180 °C, L = 25 mm, H = 1 mm) (For details see Combeaud et al. [72])

reaches a critical value of 87 s^{-1} (Fig. 29B), the fringes start to oscillate regularly, perpendicularly to the flow direction. The times t_1 and t_2 in Fig. 29 correspond to the two extreme fringe positions in the reservoir. In this situation, the melt flow coming from the reservoir enters the contraction asymmetrically. This phenomenon clearly shows the volume instability as a consequence of the flow destabilization at the die inlet, and not as a destabilization of the flow inside the channel. Moreover, as the volume instability develops further with increasing flow rate, the fringe oscillation amplitude also increases, as can be seen by comparing fringe positions from Figs. 29B and 29C. The onset of volume instability is shown on the flow curve in Fig. 29 and, as in the case of capillary experiments, onset occurs at position where there is a change in the slope of the curve which is in agreement with other reports in the literature.

For the critical apparent wall shear rate of 87 s^{-1}, (volume instability onset), the fringes movement is regularly periodic (around 0.4 Hz). When the flow rate is increased further the oscillation frequency remains essentially independent of the imposed flow rate. For larger flow rates, the frequency increases (around 0.59 Hz), but the movement loses its periodicity and the frequency fluctuates with time. For even larger flow rates (328 s^{-1}), there is an amplification of the phenomenon. The fringe displacements become more rapid and more complex and several additional modes of oscillation occur superimposed on the primary one.

By using an axisymmetric channel connected to a parallelepiped slit reservoir, *Combeaud* [68] showed that helical distortions observed at the die exit can be directly correlated with the appearance of a periodicity in the upstream FIB pattern and the instability frequency at the die exit was the same as that for the FIB oscillations. The frequency was not damped down during the flow along the die channel.

In order to quantitatively follow upstream velocity fluctuations laser-Doppler velocimetry (LDV) can be used to follow velocity changes along the symmetry axis of the slit geometry in the entry region. By choosing a position 10 mm upstream of the slit entrance as shown in Fig. 30 it was possible to monitor the time dependence of the velocity components as a deviation angle α from the symmetry axis. When periodic oscillations of the FIB were observed, a matching periodic oscillation of the angle α was also measured as shown in Fig. 30 [73]. For stable flow conditions, the angle α is obviously equal to zero. The dashed line in Fig. 30 is an interpolation of the calculated values: a(t) using a cubic spline in order to estimate the periodicity of the oscillations. Due to the noise of the velocity signals and the fluctuations of the melt supply, the shape of the interpolation is not perfectly sinusoidal. The results show that the period of oscillation for the birefringence and the velocity fluctuations are the same and clearly the instability can be correlated with the periodic upstream non axial velocity fluctuation.

The geometry of upstream extrusion die also has a significant effect on stress levels within the upstream reservoir and this is illustrated with FIB photographs in Fig. 31 for a sufficiently low flow condition where steady flow occurs. For the same flow rate it can be seen that there are many more fringes visible in Fig. 31A which is the 90 degree entrance angle. As

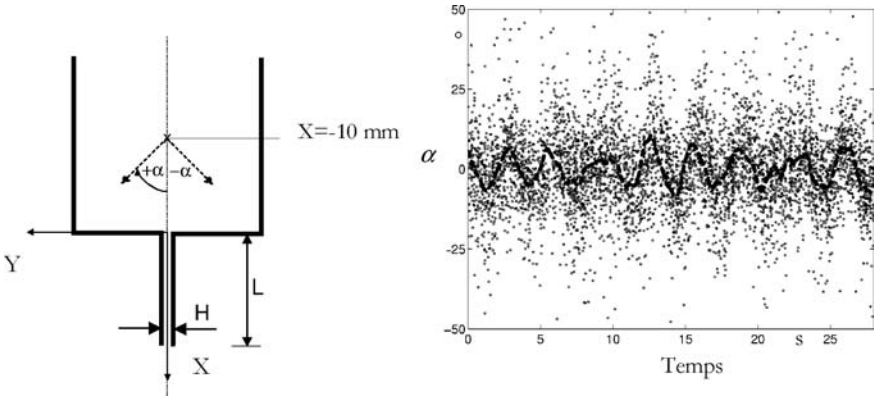

Fig. 30. Oscillation of the velocity signal at z = –10 mm (For details see Combeaud et al. [73])

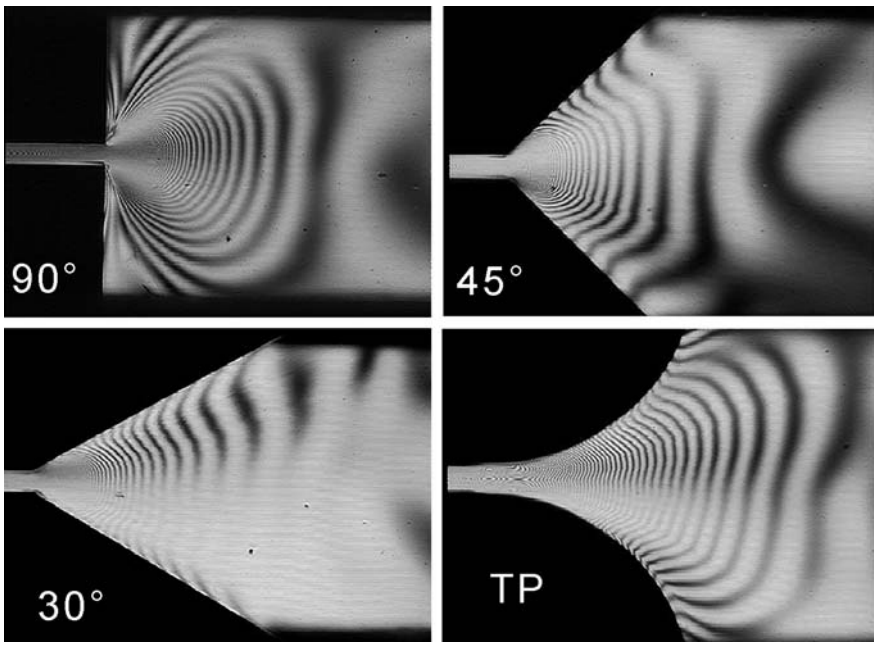

Fig. 31. FIB patterns for polystyrene in stable flow conditions for the different entrance geometries (For details see Combeaud et al. [72])

the entrance angle is reduced so too are the number of fringes and the way in which the entry extensional stress in the central region of the die develops. The effect is shown quantitatively in Fig. 32 where the centre line stress build-up and relaxation is plotted as a function of position. In the case of the 90 degree entrance angle, the stress build-up is rapid and large. As the entry angle is reduced the magnitude of the maximum stress is reduced and also the stress builds up more gradually. Both these effects are believed to influence the onset of instabilities and experimentally it is found that the onset of upstream instabilities is delayed by reducing the entry angle of the upstream region (see Fig. 33B).

5.3 Interpretation of Volume Instabilities

The results presented in this paper support the evidence that the periodic volume instabilities are initiated at the die entry. There are a number of published explanations as to the origin of the instabilities. *Den Otter* [66], *Spencer* and *Dillon* [74] and *Agassant* et al. [71] proposed that some bulk instabilities are related to unstable upstream vortices. Whilst this is true for some systems, laser-Doppler velocimetry (LDV) experiments by *Combeaud* et al. [72] showed for polystyrene that recirculation vor-

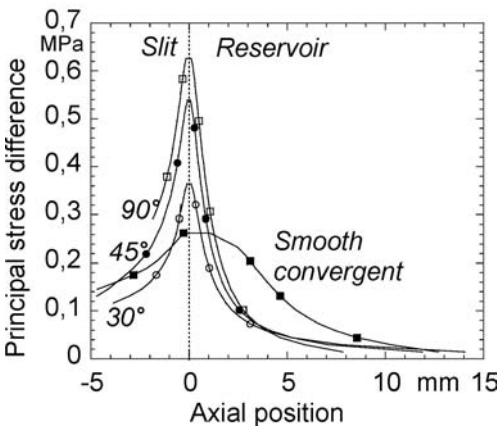

Fig. 32. Centre line principal stress difference measurements for different entrance geometries (For details see Combeaud et al. [72])

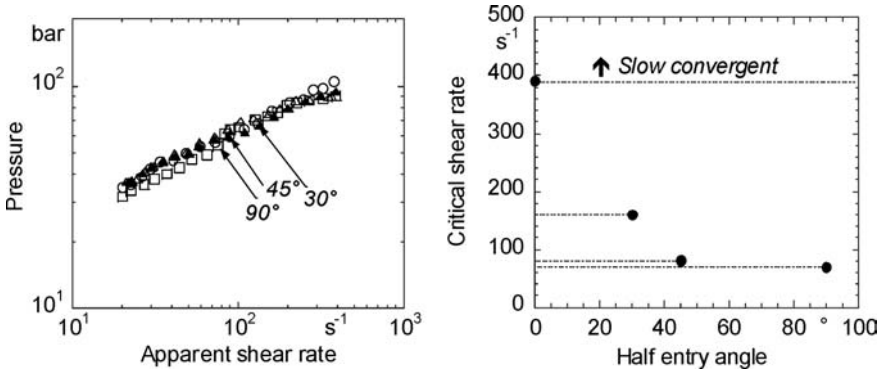

Fig. 33. (a) Apparent flow curves for the different entry half-angles, at a temperature of 180 °C. Arrows indicate the onset of volume instability. (L = 20.75 mm, ▲ = 30°, ● = 45°, □ = 90°). (b) Critical apparent shear rate as a function of convergent entry half-angle, at a temperature of 180 °C (For details see Combeaud et al. [72])

tices disappeared at entry angles of 30 or 45 degrees, but the flow still showed upstream unsteadiness.

The elongational stresses and deformations developing in the convergent have often been associated with the onset of the upstream instability [64, 65, 74]. The estimation of a critical elongational stress is difficult in the case of the slit geometry; however an estimate can be made by considering the FIB patterns obtained in stable flow conditions at a low apparent shear rate (20 s^{-1}), for the four geometries shown in Fig. 31. For all the geometries shown, along the centerline, the stresses increase in the reservoir, reach a maximum at the slit entry and then decrease along the slit. For the smooth convergent, the stress level is undoubtedly lower, compared to the other geometries. This is shown in Fig. 32 where the principal stress difference (PSD) was plotted as a function of the position along the centerline. The PSD is a maximum for the flat 90 degree entry (0.63 MPa), followed by the angles of 45° (0.54 MPa), 30° (0.36 MPa) and finally the smooth convergent (0.26 MPa). Consequently, it is seen that the shape of the convergent die plays a major role in the establishment of the extensional stress field, and that elongational stresses are largely reduced with a smooth convergent entry. This could explain the effect observed on the onset of volume instability where the condition for the onset of the upstream instability is linked to a critical extensional stress level.

Finally volume instabilities may be induced when stress levels exceed that of the melt strength as proposed by *Kim* and *Dealy* [64, 65]. At present there are therefore three plausible mechanisms for volume instabilities: instability associated with upstream recirculation, instability associated with a critical viscoelastic stress level in the entry region and finally instability associated with the mechanical rupture of the polymer in the entry region.

5.4 The Minimisation of Volume Instabilities

5.4.1 Influence of Temperature on Viscoelastic Properties

By carrying out experiments at different temperatures it has been established that the apparent shear rate at which periodic volume instabilities occurred, increased with increasing temperature [72]. The onset of the periodic instabilities in a particular slit die correlated with critical extrusion pressure as also observed for a cylindrical die [53]. Thus by increasing temperature for a particular flow rate it is possible to move out of the flow instability regime and by using simple time-temperature superposition techniques it is possible to predict the required temperature for defect free extrusion. Upstream recirculation is often associated with branched polymers and consequently a reduction in branching of the polymer may decrease the onset of instabilities. Branched polymers are often associated with long relaxation times and so the dominant effect of branching may be to increase viscoelastic stresses at any flow rate through the presence of long relaxation modes within the material.

5.4.2 Influence of the Die Converging Angle

The onset of volume instabilities is strongly influenced by the geometry of the die and data in Fig. 33 shows how the entry half angle can influence onset. The data show that the instability is not just a matter of extrusion pressure, as the pressure shear rate curve shows that onset for different geometries occurs at different entry angles. The angle itself has a profound effect with narrow angled entrance geometries showing significantly higher flow rate onset values. The observations reported here are consistent with those found already in the literature [57, 66, 75]. For the smooth convergent, the flow behaviour is different: even at the maximum flow conditions allowed by the experimental set-up (390 s^{-1}), no instability is detected. The isochromatic fringes remain completely stable even for very high pressures reached in the entry region. Such a profile then allows multiplying by at least a factor of four the critical apparent shear rate relative to the instability occurrence. It is clear therefore that there is useful scope in die design for minimising upstream instabilities.

5.4.3 Other Possibilities for Minimisation of Volume Instability

An alternative technique for instability minimisation is presented in the literature, [49, 50] and consists of introducing filters at the transition region between reservoir and die land. Again, as in the case of stick-spurt, this minimisation is created at the cost of a higher overall pressure drop. From what has been described the onset of volume instability is coupled to both geometry and polymer rheology. Modification of both molecular weight and molecular weight distribution offer considerable scope for the attenuation of viscoelasticty within the material and an associated attenuation of volume instability behaviour.

6 Discussion and Conclusions

In most cases of industrial extrusion processing the onset of extrusion instabilities controls the maximum throughput of the process and consequently the efficiency and viability of the technology. Many inter related factors influence the onset of extrusion instabilities including polymer type, polymer rheology, die geometry, surface conditions, flow rate and temperature. The key factors that control the three main extrusion instabilities have been outlined, but at present a universal engineering design protocol to predict and control extrusion instabilities still does not exist.

In some cases, especially for complex industrial flow geometries, the identification of the type of instability can be difficult as certain characteristics of sharkskin, stick-spurt and upstream instabilities can overlap; however by using specifically chosen geometries and polymers it has been possible to reveal the key features of each of the three instabilities and identify the different origin for each instability.

The sharkskin instability is a surface related instability that originates from the exit of the die and there is strong evidence to show that the instability develops as a consequence of the changing boundary conditions near the exit of the die. Within the die, polymer at the wall is either stationary or moving with a low velocity. When the polymer exits from the die, free surface boundary conditions apply and the polymer near the surface of the emerging extrudate accelerates. This local acceleration causes high extensional stresses which, if in excess of the materials melts tensile stress, can cause local fracture and the sharkskin instability.

The stick-spurt instability is also a surface related effect, but in this case the instability is linked to the stick-slip characteristics of polymer near the surface of the wall within the die. In the stick-spurt regime the polymer oscillates from conditions where wall slip does and does not occur. When slip does not happen there is an accumulation of mass and pressure within the die which is released when slip does occur. As mass flow rates vary during extrusion it is inevitable that the polymer compressibility and volume become relevant to this particular instability.

Volume instabilities have a range of mechanisms for their origin. In the most extreme case, stress levels can exceed the melt strength of the polymer and melt fracture can occur within the die. In addition the onset of recirculation zones in the upstream section of the die can promote periodic instabilities; however upstream recirculation is not essential to see instabilities and the viscoelastic behaviour of the polymer alone in the upstream region can be sufficient to initiate an unstable flow that propagates to the exit of the die and causes periodic or non periodic volume instabilities.

The paper has indicated ways in which different instabilities can be minimised and in some cases removed. In the case of the sharkskin instability it has been well known for some time that the introduction of additives has been found to be the most robust method of elimination. Detailed attention needs to be given to the exit of the region of the die and the upstream region of the die for this defect is in fact irrelevant. In the case of stick-spurt in some cases it is possible to increase temperature in order to move outside the onset regime; however in this case the key issue is the behaviour of the polymer at the near wall region of the die and both modification of the polymer itself or the wall can affect onset. Finally the volume instability can in some case be eliminated by suitable die geometry control. What is clear from these observations is that different factors affect the three different instabilities.

From what has been described, it is apparent that further insight is still required and the area remains a challenging one in terms of describing events at molecular, meso and macroscopic length scales. The basic elements of instability mechanisms have however now been established and with the advent of advanced numerical techniques it should be possible in the future to solve complex multi-variable physical problems that can quantitatively model and simulate all of the instabilities that have been described.

Acknowledgements

Most of the experimental work reported in this paper was carried out within an EU sponsored project “Postpone Polymer Processing Instabilities” (6 5RD-CT-2000-00238) and we are grateful to the EU for their financial support. The project involved the collaboration of many people both within universities and industry and we would like to acknowledge each of their collective contributions. Where ever possible we have acknowledged the work of particular researchers if their material has been used and we are most grateful for their permission to include the data within this paper. MRM wishes to thank Ecole des Mines de Paris for the opportunity to work at CEMEF Sophia-Antipolis and use time there to help prepare this paper.

References

1 *Petrie, J. C. S., Denn, M. M.:* A.I.Ch.E. J. 22, p. 209 (1976)
2 *Denn, M. M.:* Annu. Rev. Fluid Mech. 22, p. 13 (1990)
3 *Larson, R. G.:* Rheol. Acta, 31, p. 213 (1992)
4 *Wales, J. L. S.:* The application of flow birefringence to rheological studies of polymer melts, Delft University Press, Delft (1976)
5 *Arda, R. D.:* PhD Thesis, University of Cambridge (2003)
6 *Venet, C., Vergnes, B.:* J. Rheol. 41, p. 873 (1997)
7 *Arda, R. D., Mackley, M. R.:* J. Non-Newt. Fluid Mech. 126, p. 47 (2005)
8 *Keunings, R.*, in: Fundamentals of Computer Modeling for Polymer Processing. Tucker III, C.L. (Ed.), Hanser, Munich (1989)
9 *Denn, M. M.*, in: Theoretical and Applied Rheology. *Moldenaers, P., Keunings, R.* (Eds.) Proc. XIth Int. Cong. Rheology, Elsevier, New York (1992)
10 *Cogswell, F. N.:* J. Non-Newt. Fluid Mech. 2, p. 37 (1977)
11 *El Kissi, N., Piau, J. M.:* J. Rheol. 38, p. 1447 (1994)
12 *Rutgers, R. P. G., Mackley, M. R.:* J. Rheol. 44, p. 1319 (2000)
13 *Venet, C., Vergnes, B.:* J. Non-Newt. Fluid Mech. 93, p. 117 (2000)
14 *Allal, A., Lavernhe, A., Vergnes, B., Marin, G.:* J. Non-Newt. Fluid Mech. 134, p. 127 (2006)
15 *Wang, S. Q., Drda, P. A., Inn, Y. W.:* J. Rheol. 40, p. 875 (1996)
16 *Wang, S. Q., Drda, P. A.:* Macromol. Chem. Phys. 198, p. 673 (1997)
17 *Wang, S. Q., Drda, P. A.:* Rheol. Acta 36, p. 128 (1997)
18 *Molenaar, J., Koopmans, R. J., den Doelder, C. F. J.:* Phys. Rev. E. 58(4), p. 4683 (1998)
19 *Merten, A., Schwetz, M., Münstedt, H.:* Int. J. Appl. Mech. Eng. 8, p. 283 (2003)
20 *Merten, A.:* Dissertation, Universität Erlangen – Nürnberg, (2005)
21 *Merten, A., Schwetz, M., Münstedt, H.:* Proceedings of the 6th European Conference on Rheology, p. 147 (2002)

22 *Kurtz, S. J.:* Advances in Rheology, IX Intl. Congress on Rheology, Mexico, p. 399 (1984)
23 *Piau, J. M., El Kissi, N., Toussaint, F., Mezghani, A.:* Rheol. Acta 34, p. 40 (1995)
24 *Stewart, C. W.:* J. Rheol. 37, p. 499 (1993)
25 *Ghanta, V. G., Riise, B. L., Denn, M. M.:* J. Rheol. 43, p. 435 (1999)
26 *Kulikov, O., Hornung, K.:* J. Non-Newt. Fluid Mech. 124, p. 103 (2004)
27 *Yip, F., Hatzikiriakos, S. G., Clere, T. M.:* J. Vinyl Add. Tech. 6, p. 113 (2000)
28 *Migler, K. B., Lavallee, C., Dillon, M. P., Woods, S. S., Gettinger, C. L.:* J. Rheol. 45, p. 565 (2001)
29 *Arda, D. R., Mackley, M. R.:* Rheol. Acta 44, p. 352 (2005)
30 *Bagley, E. B., Cabot, I. M., West, D. C.:* J. Appl. Phys. 29, p. 109 (1958)
31 *Bagley, E. B., Birks, A. M.:* J. Appl. Phys. 31, p. 556 (1960)
32 *El Kissi, N., Piau, J. M.:* J. Non-Newt. Fluid Mech. 37, p. 673 (1990)
33 *Kalika, D. S., Denn, M. M.:* J. Rheol. 31, p. 815 (1987)
34 *Hatzikiriakos, S. G., Dealy, J. M.:* J. Rheol., 36, p. 845 (1992)
35 *Durand, V., Vergnes, B., Agassant, J. F., Benoit, E., Koopmans, R. J.:* J. Rheol. 40, p. 383 (1996)
36 *den Doelder, C. F. J., Koopmans, R. J., Molenaar, J.:* J. Non-Newt. Fluid Mech. 79, p. 503 (1998)
37 *Münstedt, H., Schmidt, M., Wassner, E.:* J. Rheol. 44, p. 245 (2000)
38 *Robert, L.:* PhD Thesis, Université de Nice Sophia-Antipolis (2001)
39 *Robert, L., Vergnes, B., Demay, Y.:* J. Non-Newt. Fluid Mech. 112, p. 27 (2003)
40 *Robert, L., Demay, Y., Vergnes, B.:* Rheol. Acta 43, p. 89 (2004)
41 *Molenaar, J., Koopmans, R. J.:* J. Rheol. 38, p. 99 (1994)
42 *Adewale, K. P., Leonov, A. I.:* Rheol. Acta 36, p. 110 (1997)
43 *Georgiou, G. C., Crochet, M. S.:* J. Rheol. 38, p. 639 (1994)
44 *Dubbeldam, J. L. A., Molenaar, J.:* J. Non-Newt. Fluid Mech. 112, p. 217 (2003)
45 *Mehtar, V., Archer, L. A.:* Macromol. 31, p. 8607 (1998)
46 *Yarin, A. L., Graham, M. D.:* J. Rheol. 42, p. 1491 (1998)
47 *Tchesnokov, M. A., Molenaar, J., Slot, J. J. M.:* J. Non-Newt. Fluid Mech. 126, p. 71 (2005)
48 *Done, D. S., Baird, D. G., Average, A. E.:* Chem. Eng. Comm. 21, p. 293 (1998)
49 *Piau, J. M., Nigen, S., El Kissi, N.:* J. Non-Newt. Fluid Mech. 91, p. 37 (2000)
50 *Goutille, Y., Majesté, J. C., Tassin, J. F., Guillet, J.:* J. Non-Newt. Fluid Mech. 111, p. 175 (2003)
51 *Ramamurthy, A. V.:* J. Rheol. 30, p. 337 (1986)
52 *Koran, F., Dealy, J.:* J. Rheol. 43, p. 1291 (1999)
53 *Combeaud, C., Demay, Y., Vergnes, B.:* Rhéologie 4, p. 50 (2003)
54 *Tordella, J. P.:* J. Appl. Phys. 27, p. 454 (1956)
55 *Benbow, J. J., Lamb, P.:* S.P.E. Trans. 3, p. 7 (1963)
56 *Piau, J. M., El Kissi, N., Tremblay, B.:* J. Non-Newt. Fluid Mech. 34, p. 145 (1990)
57 *Ballenger, T. F., Chen, I. J., Crowder, J. W., Hagler, G. E., Bogue, D. C.,White, J. L.:* Trans. Soc. Rheol. 15, p. 195 (1971)
58 *Muller, R., Vergnes, B.*, in: Rheology for Polymer Processing. *Piau, J. M., Agassant, J. F.* (Eds.), Elsevier, New York (1996)
59 *Tordella, J. P.:* Trans. Soc. Rheol., 1, pp. 203 (1957)
60 *Oyanagi, Y.:* Appl. Polym. Symp. 20, p. 123 (1973)
61 *Nakamura, K., Ituaki, S., Nishimura, T., Horikawa, A.:* J. Text. Eng. 36, p. 49 (1987)
62 *Rothstein, J. R., McKinley, G. H.:* J. Non-Newt. Fluid Mech. 98, p. 33 (2001)
63 *Nigen, S., El Kissi, N., Piau, J. M., Sadun, S.:* J. Non-Newt. Fluid Mech. 112, p. 177 (2003)
64 *Kim, S., Dealy, J. M.:* Polym. Eng. Sci. 42, p. 482 (2002)
65 *Kim, S., Dealy, J. M.:* Polym. Eng. Sci. 42, p. 495 (2002)
66 *Den Otter, J. L.:* Plast. Polym. 38, p. 155 (1970)
67 *Tordella, J. P.*, in: Rheology, *Eidrich, F. R.* (Ed.). Academic Press, New York (1969)
68 *Combeaud, C.:* PhD thesis, Ecole des Mines de Paris (2004)
69 *Bergem, N.:* Proceeding of 7th Congress in Rheology, Göteborg, p. 50 (1976)
70 *Baik, J. J., Tzoganakis, C.:* Polym. Eng. Sci. 38, p. 274 (1998)
71 *Agassant, J. F., Avenas, P., Sergent, J. Ph., Vergnes, B., Vincent, M.:* La mise en forme des matières plastiques, Lavoisier, Tec et Doc, Paris (1996)
72 *Combeaud, C., Demay, Y., Vergnes, B.:* J. Non-Newt. Fluid Mech. 21, p. 175 (2004)
73 *Combeaud, C., Vergnes, B., Merten, A., Münstedt, H.:* submitted to J. Rheol. (2006)
74 *Spencer, R. S., Dillon, R. E.:* J. Colloid Sci. 3, p. 163 (1948)
75 *Bagley, E. B., Schreiber, H. P.:* Trans. Soc. Rheol. 5, p. 341 (1961)

Date received: July 4, 2005
Date accepted: January 10, 2006